

IDENTIFICATION OF SOIL-FOUNDATION IMPEDANCE FUNCTION FROM SEISMIC RESPONSE SIGNALS OF INSTRUMENTED BUILDINGS

S. Farid Ghahari, Fariba Abazarsa, and Ertugrul Taciroglu

Department of Civil and Environmental Engineering
University of California, Los Angeles, CA

Abstract

Substructure method is generally used in engineering practice to take Soil-Structure Interaction (SSI) effects into account in seismic design. In this method, soil is modeled using discrete spring elements—Impedance Functions (IF)—that are attached to the superstructure; and the Foundation Input Motions (FIMs) are applied at the remote ends of these springs. While the application of the substructure method is simple and its computational costs are low, the determination of FIMs and the IFs are generally quite challenging. In the present study, we present a new approach to identify IFs and FIMs from response signals recorded during earthquakes. To do so, we use a flexible-based Timoshenko beam model to represent the structure and its soil-foundation system and updated the parameters of this model such that its responses match real-life data. The impedance functions of a large set of instrumented buildings are identified using this novel method and compared against various analytical solutions. Additionally, a computer program named CSMIP-CIT is developed that automatically extracts data for selected buildings in the CSMIP database and applies the method developed in this study.

Introduction

Soil- Structure Interaction (SSI) has been a research subject for more than 40 years (Jennings & Kuroiwa, 1968; Richat, 1975; Wolf, 1976). SFSI effects can be classified into two distinct effects: *kinematic* and *inertial* (Wolf & Deeks, 2004). Foundation's stiffness and distinct geometry alter earthquake excitations experienced by the system, dubbed the Foundation Input Motions (FIMs), which are different from the Free-Field Motions (FFM)s that would have been recorded in the absence of the foundation. Inertial interaction effects are due to the mass of the foundation-superstructure system, which imparts inertial forces onto the surrounding soil and causes the foundation to experience a response different from the FIM. Due to the inertial effects, the vibrating structure operates as a wave source and alters the wave field around the foundation system. Consequently, motions should be recorded adequately away from the structure to be qualified as FFM (Abrahamson *et al.*, 1991).

The *direct* and the *substructure* methods are two approaches used for taking SSI effects into account in seismic response analyses. In the direct method, a Finite Element (FE) model of the complete soil-structure system is created wherein the soil medium is represented as a semi-infinite domain (Pak & Guzina, 1999; Rizos & Wang, 2002). Due to its labor-intensive finite element model development and computational cost, the direct method is typically avoided in engineering practice. In the substructure method, the SSI problem is decomposed into three

distinct parts that are combined to formulate the complete solution (Stewart *et al.*, 1998). These three parts are (i) estimation of FIMs, (ii) determination of the frequency-dependent soil-foundation Impedance Functions (IFs), and (iii) dynamic analysis of the super-structure supported on a compliant base represented by the IFs and subjected to the FIMs (Wolf & Deeks, 2004).

Accurate estimation of FIMs and IFs control the accuracy of the substructure method. However, available formulations for estimation/determination of FIMs and IFs are primarily limited to analytical and numerical studies (Gazetas, 1983; Iguchi & Luco, 1981; Çelebi *et al.*, 2006) and experimental data (Tileylioglu *et al.*, 2010), which only represent simple cases—e.g., surface circular foundation on homogenous half space. Motivated by this, we seek here a robust and broadly applicable method to identify IFs and FIMs from earthquake-induced response signals recorded on instrumented buildings, because such data actually represents full-scale experimental data with actual environmental conditions. Recently, we have devised two distinct approaches for this purpose, dubbed *Tier A*, which involves the identification of a frequency-dependent IF from several modes of a multi-degree-of-freedom structure (tall building), and *Tier B*, which involves investigating the frequency-dependency using a large number of buildings, but concentrating on the fundamental mode.

In Tier A, the superstructure is modeled with relatively high detail using the Finite Element (FE) method. This is because SSI effects at higher modes are typically minor (Jennings & Bielak, 1973), and extracting that information requires a detailed representation of the super-structure. Then, the soil-foundation stiffnesses are identified such that the response of the FE model supported on soil-foundation springs match the measurements. We validated the Tier A approach through earthquake data recorded on the Millikan Library (Ghahari *et al.*, 2015a), and were able to identify soil-foundation dynamic stiffness values at several modes. Due to computational expense of Tier A, we devised the second approach—Tier B—in which the superstructure is represented by using a continuous Timoshenko beam model, which has a small number of model parameters (Tacioglu *et al.*, 2015; Tacioglu and Ghahari, 2015). Such a simplified model generally precludes the investigation of the frequency-dependency of the foundation system of a given building, but it can be easily applied to a large set of buildings. Therefore, with the Tier B approach, it was possible to investigate different classes of foundation systems' frequency-dependency by using several buildings with various fundamental frequencies, rather than by using several modes of a single building. In the present study, we introduce a new version of Tier B, which is currently implement it into a Matlab toolbox named CSMIP-CIT. In what follows, the formualtion details of the new Tier B approach are presented first. This is followed by various representative results obtained through the application of CSMIP-CIT to a large set of buildings.

Identification Methods

Dynamic Response of Timoshenko Beam Using Modal Superposition

Let's assume a Timoshenko beam on a sway-rocking foundation. Partial differential equations governing a Timoshenko beam (Timoshenko, 1921) are given by (Huang, 1961)

$$\mathbf{M}\ddot{\mathbf{v}}(x, t) + \mathbf{K} \mathbf{v}(x, t) = \mathbf{f}(x, t), \quad (1)$$

with

$$\mathbf{K} = \begin{bmatrix} GA_s \frac{d^2}{dx^2} & -GA_s \frac{d}{dx} \\ GA_s \frac{d}{dx} & EI \frac{d^2}{dx^2} - GA_s \end{bmatrix}, \quad \mathbf{M} = \begin{bmatrix} -\rho A & 0 \\ 0 & -\rho I \end{bmatrix} \quad (2)$$

$$\mathbf{v}(x, t) = \begin{bmatrix} y(x, t) \\ \alpha(x, t) \end{bmatrix} \quad (3)$$

$$\mathbf{f}(x, t) = \begin{bmatrix} P(x, t) \\ M(x, t) \end{bmatrix} \quad (4)$$

where a double dot indicates a second time-derivative. E , G , ρ , and A are the Young's and shear moduli, mass density, and section area, respectively. To consider the non-uniform distribution of shear stress on section, $A_s = \kappa A$ is used as the effective shear cross-sectional area, where κ can be assumed as 0.85 for rectangular sections (Cowper, 1966). The terms $y(x, t)$ and $\alpha(x, t)$ denote, respectively, the lateral displacement and bending-induced rotation of section with respect to the input excitations. $P(x, t)$ and $M(x, t)$ represent the distributed forces and moments, acting on the beam. For a flexible-base beam under horizontal earthquake base excitations $P(x, t) = \rho A \ddot{u}_g(t)$ and $M(x, t) = 0$ (we assume rocking ground motion is negligible). Using modal superposition (Clough & Penzien, 1975), the beam's response can be described as

$$\mathbf{v}(x, t) \approx \sum_{j=1}^n \boldsymbol{\varphi}_j(x) q_j(t) \quad (5)$$

with

$$\boldsymbol{\varphi}_j(x) = \begin{bmatrix} W_j(x) \\ \theta_j(x) \end{bmatrix} \quad (6)$$

in which $W_j(x)$ and $\theta_j(x)$ are two functions describing the j -th normal mode shapes for lateral displacement and rotation deformations, respectively. Function $q_j(t)$ denotes j -th modal coordinate, which is the relative displacement of a Single Degree Of Freedom (SDOF) system under $P(x, t)$ multiplied by the contribution factor. Eq. (5) is expressed as an approximation, because only n modes are used whereas the actual system has an infinite number of modes.

In what follows, the calculation of the aforementioned mode shapes (and natural frequencies) is briefly reviewed. Under free vibration conditions, both the lateral displacement and the bending-induced rotation are separable as $y(x, t) = W(x)T(t)$ and $\alpha(x, t) = \theta(x)T(t)$. So, Eq. (1) can be presented in the frequency domain as (Han *et al.*, 1999)

$$\mathbf{K} \begin{bmatrix} W(x) \\ \theta(x) \end{bmatrix} = \omega^2 \mathbf{M} \begin{bmatrix} W(x) \\ \theta(x) \end{bmatrix} \quad (7)$$

By solving Eq. (7), the normal mode shapes for $\omega_j < \sqrt{GA_s/\rho I}$ are¹

$$W_j(x) = c_1^j \sin(p^j \tilde{x}) + c_2^j \cos(p^j \tilde{x}) + c_3^j \sinh(q^j \tilde{x}) + c_4^j \cosh(q^j \tilde{x}) \quad (8)$$

$$\theta_j(x) = d_1^j \sin(p^j \tilde{x}) + d_2^j \cos(p^j \tilde{x}) + d_3^j \sinh(q^j \tilde{x}) + d_4^j \cosh(q^j \tilde{x}) \quad (9)$$

¹For brevity, we only present formulation for frequencies below the critical frequency. For frequencies above the critical frequency similar formulation with a few modifications are obtained.

with $\tilde{x} = x/L$, $p^j = |\text{Imag}(m_1^j)|$, and $q^j = m_3^j$. m_1^j and m_3^j are wave numbers corresponding to each mode and are calculated from following relationship

$$m_{1,3}^j = \sqrt{\frac{-(b_j^2 s^2 + b_j^2 R^2) \mp \sqrt{(b_j^2 s^2 + b_j^2 R^2)^2 - 4(b_j^4 s^2 R^2 - b_j^2)}}{2}} \quad (10)$$

with dimensionless parameters as

$$s^2 = \frac{EI}{GA_s L^2}, \quad b_j^2 = \frac{\rho A \omega_j^2 L^4}{EI}, \quad R^2 = \frac{I}{AL^2} \quad (11)$$

Unknown coefficients c_i^j and d_i^j are related parameters as

$$\begin{aligned} d_1^j &= \lambda_1^j c_2^j = \frac{1}{L} \left(\frac{b_j^2 s^2}{p^j} - p^j \right) c_2^j, & d_2^j &= \lambda_2^j c_1^j = \frac{1}{L} \left(-\frac{b_j^2 s^2}{p^j} + p^j \right) c_1^j, \\ d_3^j &= \lambda_3^j c_4^j = \frac{1}{L} \left(\frac{b_j^2 s^2}{q^j} + q^j \right) c_4^j, & d_4^j &= \lambda_4^j c_3^j = \frac{1}{L} \left(\frac{b_j^2 s^2}{q^j} + q^j \right) c_3^j \end{aligned} \quad (12)$$

To find c_i^j , we must apply the boundary conditions on the free vibration response. For the problem at hand, the shear force and bending moment at the base must be equal to the force and moment produced by the sway and rocking springs, respectively. Also, the shear force and bending moment at top of the beam must be zero. By applying these four boundary conditions, we have the following system of homogenous linear equations

$$\begin{bmatrix} (L\lambda_2^j - p^j) & k_T & (L\lambda_4^j - q^j) & k_T \\ -k_R \lambda_2^j & p^j \lambda_1^j & -k_R \lambda_4^j & q^j \lambda_3^j \\ (L\lambda_2^j - p^j) \cos(p^j) & (L\lambda_1^j + p^j) \sin(p^j) & (L\lambda_4^j - q^j) \cosh(q^j) & (L\lambda_3^j - q^j) \sinh(q^j) \\ -p^j \lambda_2^j \sin(p^j) & p^j \lambda_1^j \cos(p^j) & q^j \lambda_4^j \sinh(q^j) & q^j \lambda_3^j \cosh(q^j) \end{bmatrix} \begin{bmatrix} c_1^j \\ c_2^j \\ c_3^j \\ c_4^j \end{bmatrix} = \mathbf{0} \quad (13)$$

where the additional dimensionless parameters are given by

$$k_T = \frac{K_T}{GA_s/L}, \quad k_R = \frac{K_R}{EI/L} \quad (14)$$

To avoid trivial solutions in Eq. (13), the determinant of the matrix must be zero. Equation obtained by this constrain is dubbed the *frequency equation*, through which the natural frequencies ω_j are found. For each natural frequency, the unknown coefficients c_i^j can be obtained by solving Eq. (13) after assigning one of the c_i^j an arbitrary constant value (for example, $c_4^j = 1$).

To calculate the modal coordinates, modal orthogonally with respect to matrix \mathbf{M} (Han *et al.*, 1999) is used. Hence, $q_j(t)$ can be identified from the equation below, deduced from Eq. (1)

$$\ddot{q}_j(t) + \omega_j^2 q_j(t) = \frac{L_j^*}{m_j^*} \ddot{u}_g(t) \quad (15)$$

where L_j^* and m_j^* are respectively the generalized influence factor and mass, defined as

$$L_j^* = \rho A \int_0^L W_j(x) dx, \quad m_j^* = \int_0^L \boldsymbol{\varphi}_j(x)^T \mathbf{M} \boldsymbol{\varphi}_j(x) \quad (16)$$

Up to now, we assumed that the system has normal mode shapes—i.e., the mode shapes and undamped natural frequencies are independent from damping effects (classical damping). To consider damping, while retaining the normal mode assumption, we add a term $2 \omega_j \xi_j \dot{q}_j(t)$ to Eq. (15) to make it similar to the response of a damped SDOF system (Chopra, 2001). This damping term is equivalent to adding a $\mathbf{C} \dot{\mathbf{v}}(x, t)$ term to the matrix form of Eq. (1), in which \mathbf{C} is a matrix such that

$$\int_0^L \boldsymbol{\varphi}_j(x)^T \mathbf{C} \boldsymbol{\varphi}_k(x) dx = 2 m_j^* \omega_j \xi_j \delta_{jk} \quad (17)$$

where δ_{jk} is Kronecker delta. It is expedient to note here that we are not interested in knowing the actual form of matrix \mathbf{C} , because only the modal damping is important. We just assumed this form to make the formulation as simple as possible and to have real-valued mode shapes.

Identification Method

According to the previous section, the absolute acceleration of the building under horizontal base acceleration, which is recorded in real life, can be written as

$$\ddot{y}^t(x, t) = \sum_{j=1}^n W_j(x) \ddot{u}_g(t) \quad (18)$$

where $\ddot{q}_j(t)$ is relative acceleration of a SDOF system under $L_j^* \ddot{u}_g(t)/m_j^*$. For the proposed identification method, we assume that the absolute acceleration of a flexible-base building is available in three levels—namely, the foundation level $\ddot{y}^t(0, t)$, mid-height level $\ddot{y}^t(x_m, t)$, and roof level $\ddot{y}^t(L, t)$. According to Eqs. (15) and (18) each of these response signals can be expressed in the frequency domain as

$$\ddot{y}^t(x, \omega) = \left[\sum_{j=1}^n W_j(x) \frac{L_j^*}{m_j^*} H_j(\omega) + 1 \right] \ddot{u}_g(\omega) \quad (19)$$

with

$$H_j(\omega) = \frac{-\omega^2}{\omega_j^2 - \omega^2 + 2i\xi_j\omega_j\omega} \quad (20)$$

Accordingly, the response at the mid-height and the roof levels can be predicted by the response of the foundation level by eliminating the input excitation as in

$$\ddot{y}^t(x, \omega) = \frac{\left[\sum_{j=1}^n W_j(x) \frac{L_j^*}{m_j^*} H_j(\omega) + 1 \right]}{\left[\sum_{j=1}^n W_j(0) \frac{L_j^*}{m_j^*} H_j(\omega) + 1 \right]} \ddot{y}^t(0, \omega) \quad (21)$$

Therefore, by defining and solving a proper minimization problem, the unknown parameters of the system can be identified. This approach has been successfully used by Lignos and Miranda (2014) to identify the input motion of fixed-base structures who linked shear and flexural beams to represent their parametric model. We define the following optimization problem here

$$\min_{\bar{b}, s, k_T, k_R, \xi_1, \dots, \xi_n} \left\| \ddot{y}^t(x_m, t) - \ddot{\tilde{y}}^t(x_m, t) \right\| + \left\| \ddot{y}^t(L, t) - \ddot{\tilde{y}}^t(L, t) \right\| \quad (22)$$

where $\check{y}^t(x_m, t)$ and $\check{y}^t(L, t)$ denote the response signals at mid-height and roof levels predicted by Eq. (21) and transformed to the time domain through Inverse Fourier Transform. We replace the dimensionless parameter b with \bar{b} to make it mode-independent. This optimization problem is not convex and may have several local minima. We, therefore devise constraints to decrease the possibility of being trapped in a local minimum. As the first flexible-base natural frequency can be easily detected from the Fourier spectrum of the roof response using Peak Picking, we add this information as a constraint to the optimization problem. Moreover, we start the optimization procedure with many random starting points.

Once the unknown parameters are identified by solving the optimization problem, the, unknown input motion, $\ddot{u}_g(\omega)$, can be back calculated through Eq. (19) using any of the available measured response signals. Additionally, the foundation rocking response can be estimated by converting the foundation translational response, as in

$$\ddot{a}(x, \omega) = \frac{\left[\sum_{j=1}^n \theta_j(0) \frac{L_j^*}{m_j^*} H_j(\omega) \right]}{\left[\sum_{j=1}^n W_j(0) \frac{L_j^*}{m_j^*} H_j(\omega) + 1 \right]} \check{y}^t(0, \omega) \quad (23)$$

By carrying out the optimization procedure mentioned above, the modal damping ratios of flexible-base system are identified.

To identify the pseudo-flexible and fixed base damping ratios, we can easily define optimization problems similar to Eq. (22). For the pseudo-flexible model, we can predict the response of mid-height and roof levels by analyzing a pseudo-flexible base Timoshenko beam subjected to horizontal foundation response, using Eqs. (19) and (20). In this case, all modal properties—i.e., ω_j , ξ_j , m_j^* , L_j^* , and $W_j(x)$ —must be calculated for a pseudo-flexible Timoshenko beam, while $\ddot{u}_g(\omega)$ must be $\check{y}^t(0, \omega)$. The modal properties of the pseudo-flexible base Timoshenko beam model can be easily obtained through the same approach as that used for the flexible base model, by using appropriate boundary conditions. That is, the mode shapes have the same form as Eqs. (8) and (9), but the unknown coefficients must be calculated by employing proper boundary conditions—to wit, by having zero base displacement, by equating the base moment to moment-induced in the rocking spring, and by having zero shear force and bending moment at the top. Based on these boundary conditions, Eq. (13) can be converted to

$$\begin{bmatrix} 0 & 1 & 0 & 1 \\ -k_R \lambda_2^j & p^j \lambda_1^j & -k_R \lambda_4^j & q^j \lambda_3^j \\ (L \lambda_2^j - p^j) \cos(p^j) & (L \lambda_1^j + p^j) \sin(p^j) & (L \lambda_4^j - q^j) \cosh(q^j) & (L \lambda_3^j - q^j) \sinh(q^j) \\ -p^j \lambda_2^j \sin(p^j) & p^j \lambda_1^j \cos(p^j) & q^j \lambda_4^j \sinh(q^j) & q^j \lambda_3^j \cosh(q^j) \end{bmatrix} \begin{bmatrix} c_1^j \\ c_2^j \\ c_3^j \\ c_4^j \end{bmatrix} = \mathbf{0} \quad (24)$$

All other modal properties (ω_j , m_j^* , and L_j^*) are calculated identically to the flexible base model, but by using these new frequency equations and mode shapes. The damping ratio is then identified by solving a minimization problem such that the predicted mid-height and roof level responses match the recorded responses.

To identify the fixed-base damping ratio, we use the same approach again—that is, we can predict the response at mid-height and roof levels by analyzing a fixed-base Timoshenko

beam subjected to horizontal and rocking foundation responses and by minimizing the difference between predicted and recorded signals. Note that foundation-rocking response is already predicted through Eq. (23). To predict the response of a fixed-base Timoshenko beam model under base horizontal and rocking excitations, earthquake-induced distributed inertia force $P(x, t)$ introduced in Eq. (1) is equal to $\rho A \ddot{u}_g(t) + \rho A x \ddot{\theta}_g(t)$, while $M(x, t) = \rho I \ddot{\theta}_g(t)$ (where $\ddot{u}_g(t)$ and $\ddot{\theta}_g(t)$ are the horizontal and rocking foundation accelerations in our case). So, Eq. (19) is rewritten as

$$\dot{y}^t(x, \omega) = \left[\sum_{j=1}^n W_j(x) \frac{L_j^*}{m_j^*} H_j(\omega) + 1 \right] \ddot{u}_g(\omega) + \left[\sum_{j=1}^n W_j(x) \frac{\bar{L}_j^*}{m_j^*} H_j(\omega) + x \right] \ddot{\theta}_g(\omega) \quad (25)$$

where L_j^* and m_j^* are calculated using Eq. (16) and $H_j(\omega)$ is calculated using Eq. (20), in which fixed-base mode shapes and natural frequencies must be used. \bar{L}_j^* is the generalized influence factor for rocking excitation and must be calculated as follows

$$\bar{L}_j^* = \rho I \int_0^L \theta_j(x) dx + \rho A \int_0^L x W_j(x) dx \quad (26)$$

using the fixed-base mode shapes. To calculate the fixed-base mode shapes (and natural frequencies), proper boundary conditions (zero displacement and rotation at bottom, and zero shear and moment at top) will yield to the following frequency equations

$$\begin{bmatrix} 0 & 1 & 0 & 1 \\ \lambda_2^j & 0 & \lambda_4^j & 0 \\ (L\lambda_2^j - p^j) \cos(p^j) & (L\lambda_1^j + p^j) \sin(p^j) & (L\lambda_4^j - q^j) \cosh(q^j) & (L\lambda_3^j - q^j) \sinh(q^j) \\ -p^j \lambda_2^j \sin(p^j) & p^j \lambda_1^j \cos(p^j) & q^j \lambda_4^j \sinh(q^j) & q^j \lambda_3^j \cosh(q^j) \end{bmatrix} \begin{bmatrix} c_1^j \\ c_2^j \\ c_3^j \\ c_4^j \end{bmatrix} = \mathbf{0} \quad (27)$$

Based on the identification method presented above (i.e., the Tier B approach), we developed a Matlab (2013) toolbox named CSMIP-CIT (Ghahari *et al.*, 2015b). In addition to the identification capabilities, this software offers a user-friendly graphical tools for classification of *all* buildings instrumented through the California Strong Motion Instrumentation Program (CSMIP) that are available in the Center for Engineering Strong Motion Database (CESMD)². CSMIP-CIT (Figure 1) is able to connect to the data center through Internet and download the data, and to apply the proposed identification approach.

² www.strongmotioncenter.org

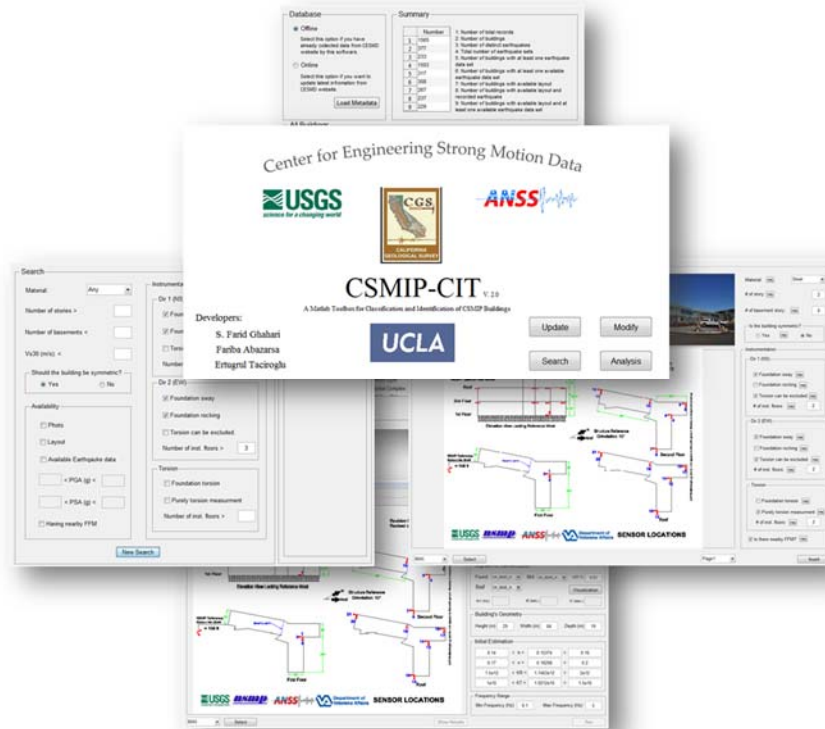


Figure 1. Graphical user interface of the CSMIP-CIT software (Ghahari *et al.*, 2015b).

A Validation Example

To validate the identification approach presented above, we use real-life earthquake data recorded on the Millikan Library. The Millikan Library—named after Robert Andrew Millikan, who is a 1923 Nobel-laureate experimental physicist—is a reinforced concrete building with a basement level and 9 stories above the ground. It is located on the campus of California Institute of Technology (Caltech) in Pasadena, California, and was constructed during 1966 to 1967. It is one of the world’s most densely instrumented buildings, and due to its structural and soil conditions, it has been the subject of numerous studies on soil-structure interaction (see, for example, Jennings & Kuroiwa, 1968; Luco, *et al.*, 1988; Bradford, *et al.*, 2004; Snieder & Safak, 2006; Todorovska, 2009; Cheng & Heaton, 2013). We have recently analyzed the response signals of the Millikan Library recorded during the 2002 Yorba Linda earthquake using a new blind modal identification method (Ghahari *et al.*, 2015a). Significant soil-structure interaction effects in the North-South (NS) direction have been already detected by many researchers (e.g., Todorovska, 2009). So, we use the signals and the identified modal properties of this particular direction here, for comparisons.

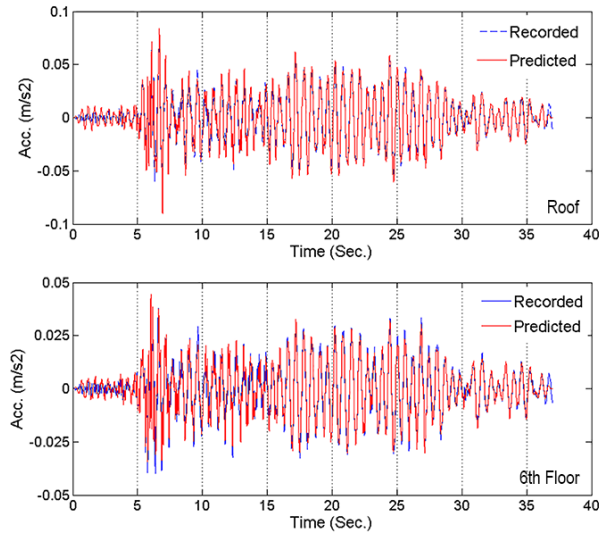


Figure 2. Comparison between response signals recorded and predicted.

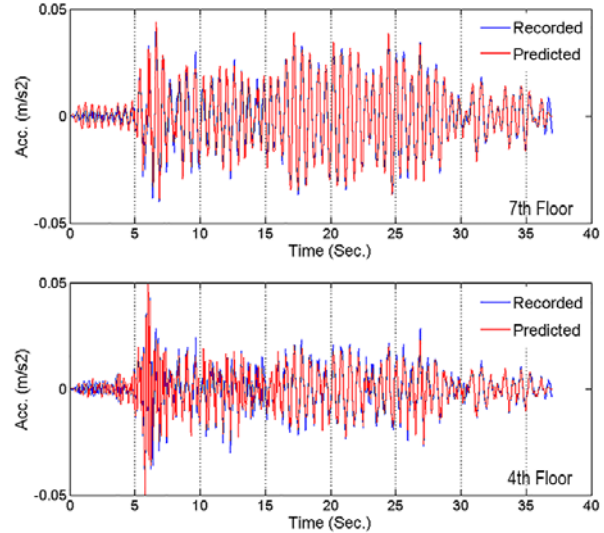


Figure 3. Comparison between response signals recorded and blindly predicted.

By using only the acceleration signals recorded on the foundation (sway), 6th floor, and the roof, the unknown parameters of flexible-base Timoshenko beam model are identified first. Figure 2 displays the recorded and predicted acceleration signals. There is a very good agreement, but it is not surprising, because both signals are used in the objective function of the minimization procedure. Figure 3 shows results of a blind prediction of the responses at two other floors. As seen, the same level of agreement is observed for these two floors. Multiplying the identified mass normalized sway and rocking stiffness parameters with the estimated mass of the Millikan Library (Ghahari *et al.*, 2015a), the soil-foundation sway and rocking stiffnesses are obtained as 1.89×10^{10} N/m and 2.32×10^{12} N, respectively. Using the identified stiffnesses from the Tier A approach (Ghahari *et al.*, 2015a) as reference values, the newly identified stiffnesses have 17% and 13% relative errors, respectively. As CSMIP-CIT identifies a frequency-independent soil-foundation impedance function, it is expected to exhibit larger errors/variability in comparison with Tier A, with which the soil-foundation stiffnesses were identified for each mode separately. Also, the larger error of sway stiffnesses is due to the fact that foundation sway relative to the soil is negligible for this particular building.

Finally, the natural frequencies of identified model with two different base-fixity conditions (i.e., flexible and fixed) are shown in Table 1 and compared with identified and FE model values. As seen, the two first flexible-base modes are almost identical to the identified and Tier A values. The source of difference in third mode's natural frequency of the flexible-base model is described in Taciroglu *et al.* (2015). Results in Table 1 also indicate that the first fixed-base natural frequency of both Tier A and the identified Timoshenko beam model are identical to the identified value.

The damping ratios of the Millikan Library have not been identified in any prior studies from earthquake data. Through application of CSMIP-CIT, these values for three base-fixity conditions are identified here. As there is negligible foundation sway, the first mode's damping ratios of both flexible- and fixed-base models are 1.62%, while for the fixed-base model, it is

2.34%. Indeed, foundation rocking could not compensate the reduction in the overall damping ratio, which is caused by a decrease in the natural frequency of the system that occurs due to the soil-foundation-system’s hysteretic and radiation damping.

Table 1. Natural frequencies identified using different methods.

Mode No.	Flexible-base System			Fixed Base System		
	Identified	FE Model	CSMIP-CIT	Identified	FE Model	CSMIP-CIT
1	1.68	1.68	1.68	2.05	2.07	2.04
2	6.64	6.64	6.71	---	7.51	7.14
3	12.48	12.53	13.87	---	13.96	14.63

Application to CSMIP Data

Data Classification

In this section, results obtained through the application of CSMIP-CIT to building data available in the CESMD database are presented. Table 2 displays a summary of available building data in the aforementioned database. This classification is carried out by the *classification* capabilities of the developed software. As seen in Table 2, from among 381 instrumented buildings, only 234 can be studied at the present time due to the availability of both instrumentation layouts and earthquake data.

Table 2. Available building data in CESMD (Last update: 10/02/2015)

Item Description	Number
Number of total records	1604
Number of buildings	381
Number of earthquakes	240
Number of earthquake sets	1541
Number of buildings with at least one earthquake	320
Number of buildings with at least one available earthquake	312
Number of buildings with available layout	269
Number of buildings with available layout and at least one recorded earthquake	241
Number of buildings with available layout and at least one available earthquake	234

Material distribution of 381 buildings is shown in Figure 4(a). As seen, metadata of 35% (135) of the buildings are not available (there are 23 buildings that have instrumentation layouts, but it is not possible to determine their material type through CESMD). A similar plot for buildings with instrumentation layout and available earthquake data is given in Figure 4(b). As seen, more than 74% of such buildings have steel or concrete lateral resisting systems, and feature no seismic isolation devices. We concentrate on these buildings in the current study, of which there are 174.

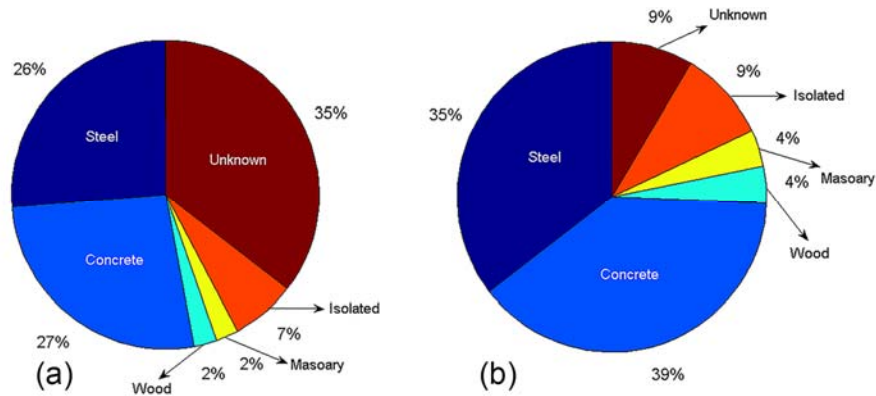


Figure 4. Material distribution of (a) all 381 instrumented buildings, and (b) 234 buildings with available earthquake data and instrumentation layout.

Theoretically, soil-foundation flexibilities can be identified by investigating the difference between the so-called flexible-based and fixed-base system’s properties (Stewart *et al.*, 1999a, b). To identify both the fixed- and flexible-base properties, the FFM, foundation sway, foundation rocking, and building responses must be measured (Stewart, 1996). However, the number of CSMIP buildings with necessary instrumentation for this purpose is very limited. As shown in Figure 5 under Case 1, among the 174 selected buildings, the total number of steel and concrete buildings that have instrumentation layouts, available earthquake records, nearby Free-Field Motion (FFM) stations, foundation sway and rocking instrumentations, and at least one instrumented floor is less than 10 (out of the selected 174 buildings)! Note that it is actually possible to find FFM stations close to some of other buildings, but the aforementioned classification is based on FFM stations shown on the instrumentation layouts available in CESMD. If we can relax this requirement, then the number of specimen buildings increases to 25 (denoted as Case 2). Such a number is still very small and cannot be used to extract aggregate results from which broad conclusions can be drawn.

Another critical limitation is the availability of the foundation rocking measurement. By relaxing this condition as well, the number of buildings increases from 25 to around 170 (denoted as Case 3). Having only one sensor on the structure may not capture contribution of different modes. Therefore, it is more favorable to have additional sensors. As the figure shows, by adding one more sensor as an additional requirement (denoted as Case 4), the number of buildings available for study decreases³, but not significantly (~152). Based on this, we designed CSMIP-CIT for Case 4 —i.e., we analyzed 152 instrumented buildings.

From the 152 candidates e, we gave priority to buildings that have (1) symmetric plans, and uniform mass and stiffness distributions along their height; (2) *several* recorded earthquakes; and (3) known soil shear wave velocity values. These properties helped us to be able to use the Timoshenko beam theory, to make sure that the identified results were consistent, and to combine dynamic foundation stiffness values identified from different buildings in a consistent manner. According to these criteria, 66 buildings with a total of 279 earthquake data sets were

³ Requiring one additional sensor beyond that would reduce this number to 105.

analyzed. These buildings were classified according to their lateral resisting systems into three groups as shown in Figure 6.

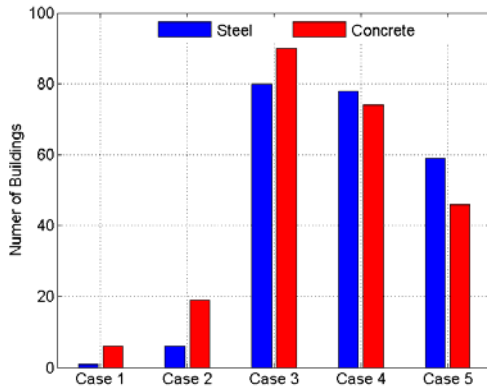


Figure 5. Number of instrumented buildings for various instrumentation scenarios.

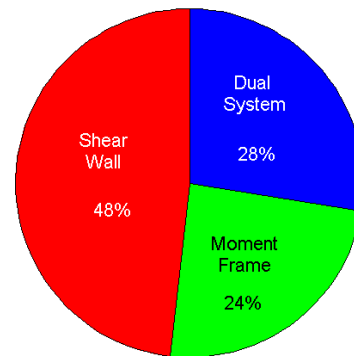


Figure 6. Distribution of chosen buildings according to their lateral system type.

Superstructure Parameters

The algorithm designed for CSMIP-CIT is able to identify the super-structure parameters, the soil-foundation system’s sway and rocking stiffnesses, as well as natural frequencies and modal damping ratios of the entire system for flexible-, pseudo-flexible, and fixed-base conditions. Figure 7 shows the shear wave velocity of the buildings, $\sqrt{G/\rho} = L/(\sqrt{k_s b})$. As seen and expected, buildings with shear wall and moment frame systems have the highest and lowest values of wave velocity, respectively. Note that the structural nonlinearity is implicitly included in this figure, because results from various earthquakes with various levels of excitations have been used.

Building damping ratio is one of the challenging parameters to estimate in earthquake engineering, as it is not directly computable and many factors contribute to it. As such, identification of damping values from vibration data is the only viable path to quantification. As summarized by Bernal *et al.* (2013), several researchers suggested simplified formulae for first mode damping ratios using different parameters and calibrated these by using damping ratios estimated/identified from vibration data. Building height, material type, and vibration intensity were utilized as the primary physical parameters. There has been no discussion about the amplitude-dependency of the damping ratios. Bernal *et al.* (2013) also stated that there is no direct correlation between the damping ratio and the natural frequency. Indeed, taller buildings (having lower natural frequency) have higher aspect ratios, so the damping provided by the soil would be less, and consequently the overall damping ratio would be less. Based on this conjecture, they suggested an empirical formula for the first mode damping ratio using the building height and the material type (Bernal *et al.*, 2015). Their conjecture may indeed be true; nevertheless, Bernal *et al.* (2013) have only identified the pseudo-flexible damping ratio, because they have used the foundation sway as input in their input-output identification study. Therefore, foundation rocking may alter the overall damping ratio due to hysteretic and radiation damping

that the soil-foundation interface nominally exhibits (the same statement is true for the natural frequency). In our approach, it is possible to exclude the soil-foundation system's effects and to identify the natural frequency and damping ratio of the superstructure itself.

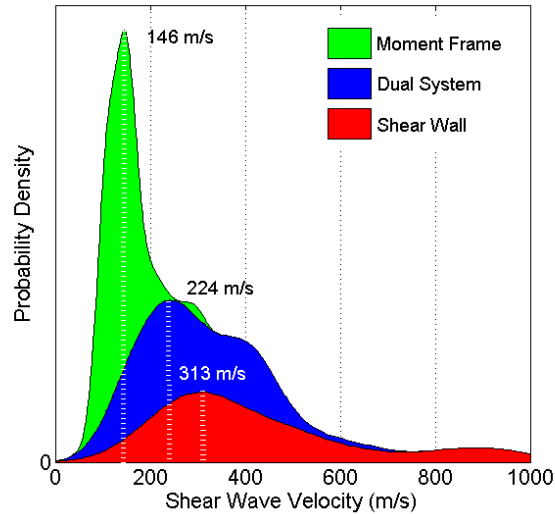


Figure 7. Probability distribution of shear wave velocity in fixed-base buildings.

Figure 8 displays the identified fixed-base natural frequencies and damping ratios of all 279 cases. Histograms of the identified values are also shown alongside. According to this figure, we can state:

1. Fixed-base natural frequencies of shear-wall buildings have higher variances (note that amplitude-dependency is included) in comparison to moment-frame systems. This is expected because natural frequencies of shear-wall buildings are more sensitive to cracking than moment frame systems.
2. Contrary to the natural frequency, damping ratio behaves in the reverse manner. That is, the variation of damping ratios in moment-frame systems is higher, probably because of the direct relationship between friction in connections and the level of vibrations.
3. There is a direct relationship between the damping ratio and the natural frequency. In stiffer systems, more elements are interacting with each other, and thus the damping level should be higher. Also, the slope of variation for moment-frame structures is greater than that for shear wall systems.

We do not present any regression results here, because it is out of scope of the present study. However, by excluding the amplitude-dependency from the identified results, it appears possible to reach a more realistic empirical formula for damping prediction of buildings.

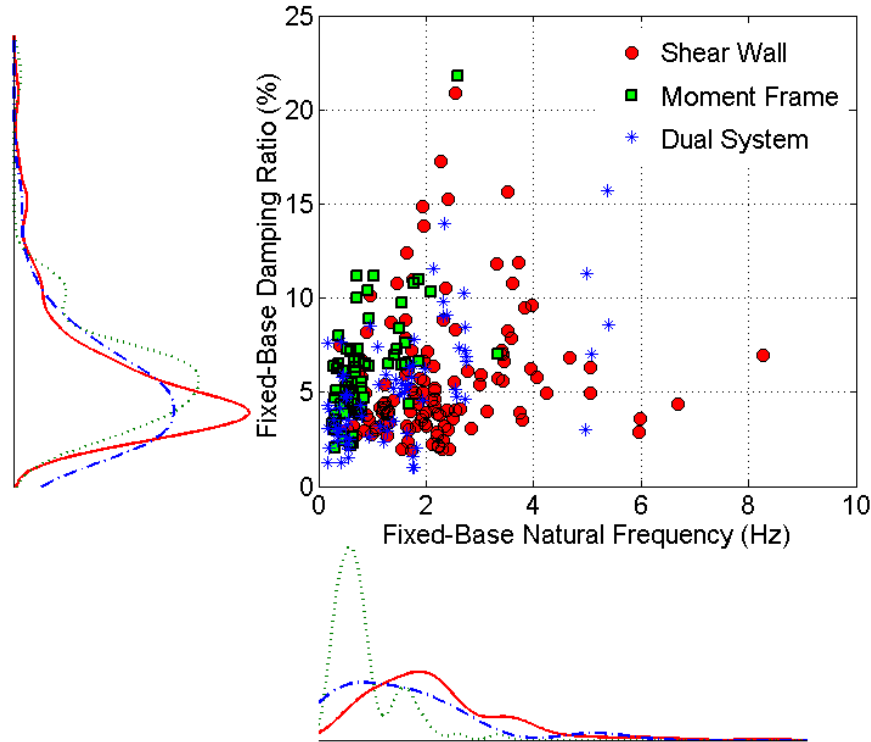


Figure 8. Variation of the fixed-base damping ratio versus fixed-base natural frequency.

Soil-Foundation Parameters: Frequency-Dependency

Here, the identified flexible-base modal properties are compared with available models. Period elongation and foundation damping are two parameters that are used in design codes for considering soil-structure interaction effects (e.g., ASCE-7, 2010). Figure 9(a) displays the period elongation—which is the ratio of the identified flexible-base to the fixed-base natural periods ($T_{Flexible}/T_{Fixed}$)—versus a dimensionless measure of the structure-to-soil stiffness—i.e., $h/(V_s T_{Fixed})$ where h is effective height, V_s is effective soil's shear wave velocity, and T_{Fixed} is fixed-base fundamental natural period. For comparison, the theoretical results derived by Veletsos and Nair (1975) for rigid surface circular foundation with 10% soil material damping and for three structural aspect ratios are shown. Circles shown in this figure denote results for a subgroup of the 66 buildings for which the identified flexible- and fixed-base natural periods are different (i.e., they exhibit inertial SSI effects). To calculate the aspect ratio of each building, their rectangular foundations (footprint of the building) are approximated by their equivalent circular foundation (Wolf and Deeks, 2004) and 70% of the height of the building is used as the effective height. For buildings that have already been studied by Stewart and Stewart (1997), the same earthquake data are used, so that the effective V_s values can be directly taken from their study. In cases where effective V_s was not available, earthquakes with minimum Peak Ground Acceleration (PGA) and V_s reported by Seyhan *et al.* (2014) were used. In the absence of small PGA earthquakes, V_s was reduced according to Table 4-1 of National Institute of Standards and Technology (NIST).

As seen in Figure 9(a), considering all available uncertainties (embedding, shear wave velocity, nonlinearity, etc.), the theoretical model by Veletsos and Nair (1975) produces good predictions. A similar graph for foundation damping is shown in Figure 9(b). Foundation damping is identified as the difference between flexible-base damping ratio and fixed-base damping ratio reduced by a factor of $(T_{Flexible}/T_{Fixed})^3$. This graph indicates that the theoretical model overestimates the foundation damping for most cases. Finally, foundation damping is presented versus period elongation in Figure 9(c). Similar graph is currently used in ASCE-07 (2010). Again current formula overestimates foundation damping for a specific period elongation.

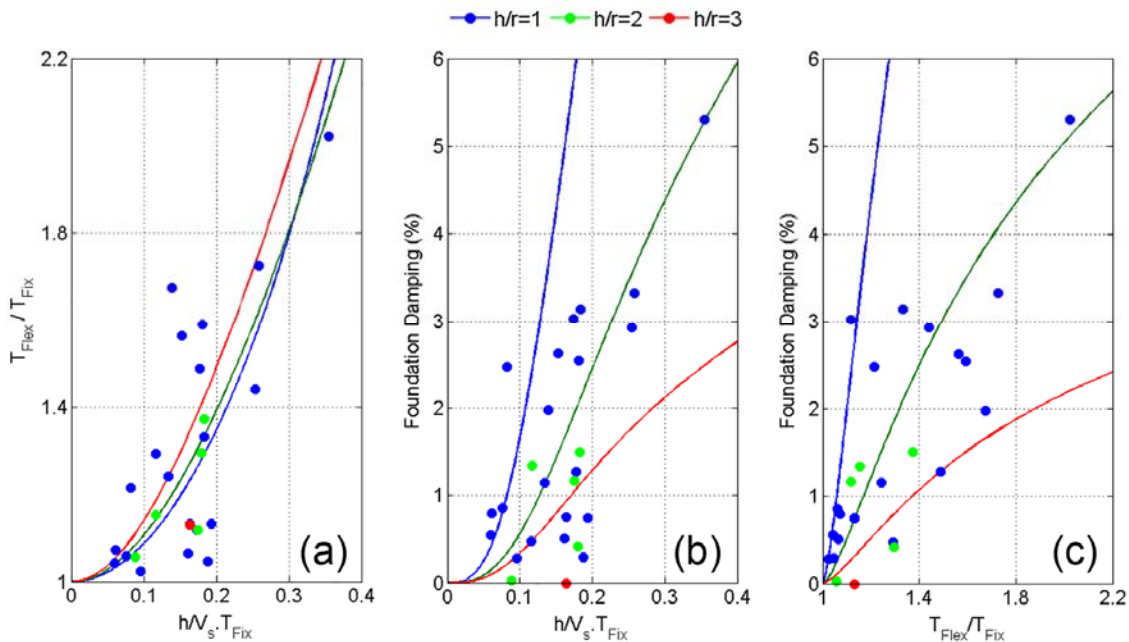


Figure 9. Comparison between identified (symbols) period elongation and foundation damping values with those predicted using the model by Veletsos and Nair (1975) (solid lines).

By selecting those buildings for which the identified fixed-base and pseudo-flexible-base natural frequencies are different, it is possible to investigate the frequency-dependency of the soil-foundation rocking stiffness. To do so, the identified stiffnesses are multiplied by an estimation of the buildings' masses and are normalized by the theoretically calculated static stiffnesses (Wolf and Deeks, 2004). Frequency-dependent impedance functions are typically presented versus the dimensionless parameter $a_0 = \omega r/V_s$. For each building, a_0 is calculated at its fundamental flexible-base natural frequency. The equivalent radius of the foundation (r) and soil's shear wave velocity (V_s) were discussed earlier. The extracted frequency-dependent rocking stiffnesses are shown in Figure 10 as single points. For comparison, a theoretical curve proposed by Veletsos and Verbic (1973) is also shown. The identified values are denoted using four different symbols. There were two buildings for which the results are not close to the theoretical values, and these are suspected to have flexible foundation systems (Stewart and Stewart, 1997). For another three buildings, we could not find strain-compatible shear wave velocity values. Finally, there were two buildings that were also far from theoretical values

due to unspecified reasons. The remaining buildings in the dataset (a majority) were interestingly in very good agreement with formula proposed by Veletsos and Verbic (1973), while noting that a Poisson's ratio of 0.45 and 10% material damping was used to generate the theoretical curve.

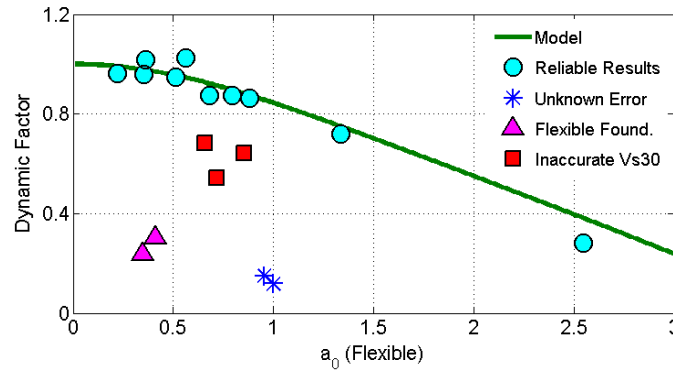


Figure 10. Identified soil-foundation rocking stiffness' frequency-dependency versus what predicted by Veletsos and Verbic (1973).

As a final result, we investigated kinematic interaction effects. Kinematic interaction has been rarely studied by solving inverse problems using real-life data. A study by Kim and Stewart (2003) is one of these rare studies; however, they extracted the Transfer Functions between the nearby FFM and the recorded foundation motions, which are not equal to FIM. By contrast, we used the true FIM here, which we could extract using identification approach proposed in this paper. As an example, Figure 11 displays the Transfer Function calculated between the FIM recovered for the 2011 Berkeley Earthquake from the transverse direction of Station 58503, and its nearby FFM station 58505. Per the recommendation by Kim and Stewart (2003), the Transfer Function is shown only for frequencies at which coherence (Pandit, 1991) is greater than 0.8. The theoretical Transfer Function for a rigid rectangular foundation with the same dimensions and shear wave velocity under vertical incoherent SH waves with incoherency factor of $\gamma = 0.5$ (Veletsos *et al.*, 1997) is also shown. As seen, while the extracted Transfer Function is jagged, its mean value follows the theoretical prediction fairly well.

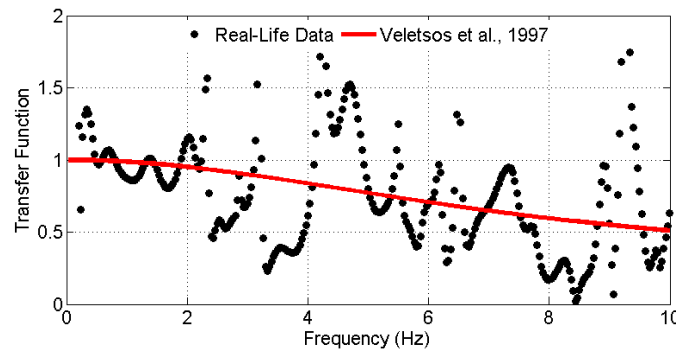


Figure 11. Comparison between the identified kinematic transfer function with that predicted through the model by Veletsos *et al.* (1997) using vertical incoherent shear wave formulation.

Soil-Foundation Parameters: Amplitude-Dependency

In the previous section, we attempted to avoid the inherent amplitude-dependency of impedance functions by using only low-intensity earthquake data or by *correcting* the soil shear wave velocities. However, soil nonlinearity is ever-present and must be well studied. As an example, the time-history and time-frequency distribution of foundation rocking and roof acceleration of CSMIP station #57356 recorded during the 1989 Loma Prieta Earthquake are shown in Figure 12. As this figure shows, there are significant temporal variations. As the large amplitude excitations arrived, the natural frequency reduced to its minimum and it gradually recovered at the end of the event. Therefore, depending on which time segment of signals are used in CSMIP-CIT, different values of impedance functions will be identified.

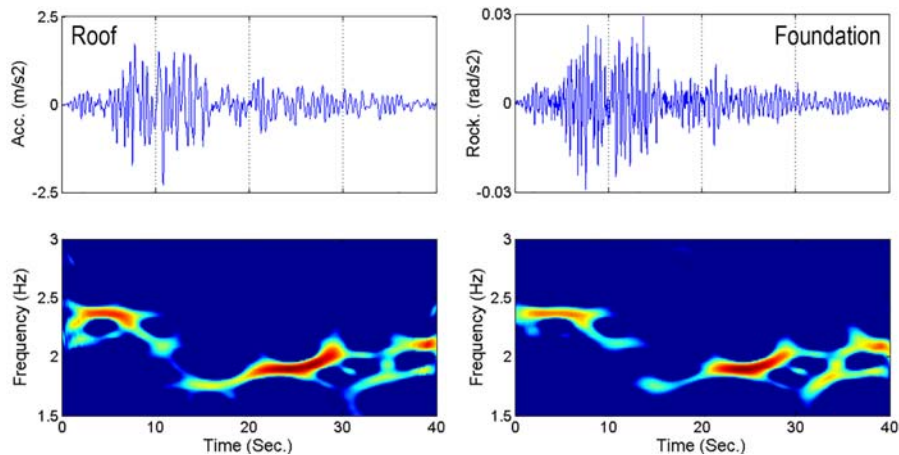


Figure 12. Time variation of the first natural frequency of CSMIP57356 during the 1989 Loma Prieta Earthquake⁴.

We carried out identification for CSMIP 57356 using several earthquake data sets. For the Loma Prieta earthquake, which was a severe event at this station, we carried out identification in four successive time segments. The identified rocking stiffnesses (mass normalized values) versus Peak Foundation Accelerations are shown in Figure 13. As seen, there is a clear amplitude-dependency. That is, the rocking stiffness decreases when the level of vibration increases. This figure also shows that the soil stiffness does not quickly recover. In other words, the identified rocking stiffnesses at the third and the final time windows for the Loma Prieta earthquake (1989) are lower than those expected for the given earthquake intensity.

⁴ Colors do not reflect the actual signal energy at each time instant, because the signal has been scaled with its instantaneous amplitude to show its instantaneous frequencies more clearly.

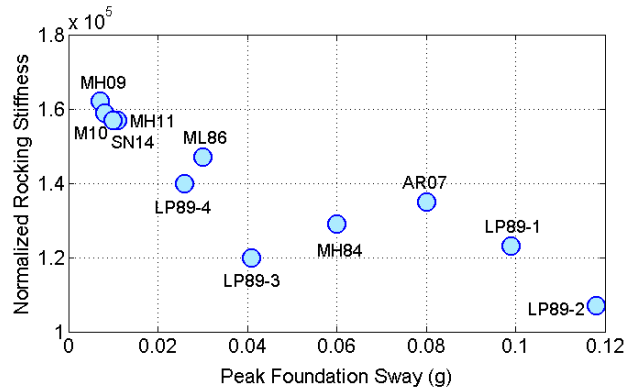


Figure 13. Amplitude dependency of the soil-foundation rocking stiffness observed at station CSMIP57356.

As a final observation, we try to see the compatibility between the amplitude-dependency of the results with those predicted by a formula usually used in practice. For this purpose, we first have to translate the peak foundation (\sim ground) acceleration to shear strain. To do so, we use following relationship between maximum shear strain and amplitude of a vertically propagating sinusoidal shear wave (Beresnev and Wen, 1996),

$$|\gamma_{max}| = \frac{A}{2\pi f V_s} \tag{28}$$

where A is the acceleration amplitude, f is the wave frequency, and V_s is the soil shear wave velocity. We use amplitude of the Fourier Transform of foundation response at first mode's flexible-base natural frequency (f) as an approximation of A . For the shear wave velocity, we use the small strain value proposed by Stewart and Stewart (1997). Figure 14 presents the same data points of Figure 13 but in different axes. The horizontal axis is now shear strain, which is calculated through Eq. (28), and the vertical axis is rocking stiffness scaled by the maximum value obtained among all data points —*viz.*, during the 2009 Morgan Hill Earthquake. For comparison, we have shown the shear reduction curve suggested by Ishibashi and Zhang (1993). The best-fit curve was obtained when we adjusted the plasticity index to 0 (i.e., sandy soil). As seen, there is very good agreement between the theoretical formula and the identified values.

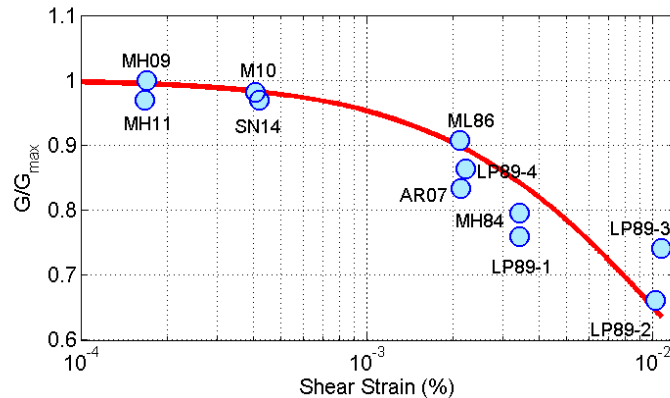


Figure 14. Soil's shear modulus reduction identified in station CSMIP57356.

Conclusions

We proposed an efficient method through which the soil-foundation systems impedance functions and foundation input motions can be identified using earthquake-induced response signals of an instrumented buildings recorded on three levels: foundation, mid-height, and roof. In this method, the building is represented with a simple Timoshenko beam model and the soil-foundation system's impedance function is estimated through an optimization problem without the need to have the foundation input motions (FIM). After identifying the flexible-base beam, the FIM is back-calculated. To facilitate broader use of this method and to simplify its application to CSMIP data, we developed a software tool, dubbed CSMIP-CIT. We used this toolbox and analyzed more than 60 buildings, which, in total, have more than 250 earthquake data sets. The results obtained so far validated some of the theoretical approximations, and also indicated that SSI effects have various intrinsic features that the soil-foundation systems of real-life structures *do* exhibit under seismic shaking, such as frequency- and amplitude-dependency. Kinematic interaction effects as well as superstructure damping values were quantified from the datasets used thus far. Broader findings will be possible once the method proposed herein is applied to more datasets.

Acknowledgments

The work presented in this manuscript was funded, in part, by the California Geological Survey (Contract No. 1014-963) and by the California Department of Transportation (Grant No. 65A0450). Any opinions, findings, conclusions or recommendations expressed in this material are those of the authors and do not necessarily reflect the views of the sponsoring agencies.

References

- Abrahamson, N.A., Schneider, J.F. & Stepp, J.C. 1991. Empirical spatial coherency functions for applications to soil-structure interaction analyses." *Earthquake Spectra*, 7(1), 1-27.
- American Society of Civil Engineers, ASCE, 2010. Minimum Design Loads for Buildings and Other Structures, Report ASCE/SEI 7-10, Reston, VA.
- Aristizabal-Ochoa, J., 2004. Timoshenko beam-column with generalized end conditions and nonclassical modes of vibration of shear beams. *Journal of Eng. Mech.*, 130(10), 1151-1159.
- Beresnev, I.A., & Wen, K. L., 1996. Nonlinear soil response—a reality?. *Bulletin of the Seismological Society of America*, 86(6), 1964-1978.
- Bernal, D., Kojidi, S.M., Kwan, K., & Döhler, M., 2013. Damping Identification in Buildings from Earthquake Records. In SMIP12 Seminar Proceedings, 39-56.
- Bernal, D., Döhler, M., Kojidi, S. M., Kwan, K., & Liu, Y. 2015. First mode damping ratios for buildings. *Earthquake Spectra*, 31(1), 367-381.
- Bradford, S., Clinton, J., Favela, T. & Heaton, T., 2004. *Results of Millikan library forced vibration testing*: Earthquake Engineering Research Laboratory.

- Çelebi, M., Firat, S. & Çankaya, I., 2006. The evaluation of impedance functions in the analysis of foundations vibrations using boundary element method. *Applied Mathematics and Computation*, 173(1), 636-667.
- Cheng, M. & Heaton, T., 2013. Simulating building motions using the ratios of its natural frequencies and a Timoshenko beam model.. *Earthquake Spectra*.
- Chopra, A., 2001. Dynamics of structures: theory and applications to earthquake engineering. 2nd ed. s.l.:Prentice-Hall.
- Clough, R. & Penzien, J., 1975. *Dynamics of Structures*, McGraw-Hill.
- Cowper, G., 1966. The shear coefficient in Timoshenko's beam theory. *ASME Journal of Applied Mechanics*, 33(2), 335-340.
- Gazetas, G., 1983. Analysis of machine foundation vibrations: state of the art. *International Journal of Soil Dynamics and Earthquake Engineering*, 2(1), 2-42.
- Ghahari, S., Abazarsa, F., Ghannad, M. & Taciroglu, E., 2013. Response-only modal identification of structures using strong motion data. *Earthquake Engineering and Structural Dynamics*, 42(8), 1221-1242.
- Ghahari, S., Abazarsa, F., Ghannad, M.A., Celebi, M. & Taciroglu, E., 2014. Blind modal identification of structures from spatially sparse seismic response signals. *Structural Control and Health Monitoring*, 21, 649-674.
- Ghahari, S., Abazarsa, F., Avci, O., Celebi, M. & Taciroglu, E., 2015a. Blind identification of the Millikan Library from earthquake data considering soil structure interaction. *Structural Control and Health Monitoring* (in press).
- Ghahari, S., Abazarsa, F. & Taciroglu, E., 2015b. *CSMIP-CIT*. V2.
- Han, S., Benaroya, H. & Wei, T., 1999. Dynamics of transversely vibrating beams using four engineering theories.. *Journal of Sound and Vibration*, 225(5), 935-988.
- IBC, 2012. *International Building Code*, Washington D.C: International Code Council.
- Iguchi, M. & Luco, E., 1981. Dynamic response of flexible rectangular foundations on an elastic half-space. *Earthquake Engineering & Structural Dynamics*, 9(3), 239-249.
- Ishibashi, I., & Zhang, X., 1993. Unified dynamic shear moduli and damping ratios of sand and clay. *Soils and Foundations*, 33(1), 182-191.
- Jennings, P. & Bielak, J., 1973. Dynamics of building-soil interaction.. *Bulletin of the Seismological Society of America*, 63(1), 9-48.
- Jennings, P. & Kuroiwa, J., 1968. Vibration and soil-structure interaction tests of a nine-story reinforced concrete building. *Bulletin of the Seism. Society of America*, 58(3), 891-916.
- Kim, S., & Stewart, J.P., 2003. Kinematic Soil-Structure Interaction from Strong Motion Recordings. *Journal of Geotechnical and Geoenvironmental Engineering*, 129(4), 323-335.
- Lignos, D. & Miranda, E., 2014. Estimation of base motion in instrumented steel buildings using output-only system identification. *Earthquake Engineering and Structural Dynamics*, 43(4), pp. 547-563.

- Luco, J., Trifunac, M. & Wong, H., 1988. Isolation of soil-structure interaction effects by full-scale forced vibration tests. *Earthquake Engineering and Structural Dynamics*, 16(1), 1-21.
- MATLAB, 2013. The language of technical computing., s.l.: Mathworks.
- National Institute of Standards and Technology, NIST (2012). Soil-Structure Interaction for Building Structures, Report NIST/GCR 12-917-21, presented by NEHRP Consultants Joint Venture, J.P. Stewart (project director), September.
- Pais, A. & Kausel, E., 1988. pproximate formulas for dynamic stiffnesses of rigid foundations.. *Soil Dynamics and Earthquake Engineering*, 7(4), 213-227.
- Pak, R. & Guzina, B., 1999. Seismic soil-structure interaction analysis by direct boundary element methods. *International Journal of Solids and Structures*, 36(31), 4743-4766.
- Pandit, S.M., 1991. Modal and Spectrum Analysis: Data Dependent Systems in State Space. Wiley-Interscience.
- Richart, F., 1975. Some effects of dynamic soil properties on soil-structure interaction. *Journal of the Geotechnical Engineering Division (ASCE)*, 101(2), 1193-1240.
- Rizos, D. & Wang, Z., 2002. Coupled BEM-FEM solutions for direct time domain soil-structure interaction analysis. *Engineering Analysis with Boundary Elements*, 26(10), 877-888.
- Seyhan, E., Stewart, J.P., Ancheta, T.D., Darragh, R.B., & Graves, R.W., 2014. NGA-West2 site database. *Earthquake Spectra*, 30(3), 1007-1024.
- Snieder, R. & Safak, E., 2006. Extracting the building response using seismic interferometry: Theory and application to the Millikan Library in Pasadena, California. *Bulletin of the Seismological Society of America*, 96(2), 586-598.
- Stewart, J.P. 1996. An empirical assessment of soil-structure interaction effects on the seismic response of structures. Doctoral dissertation, University of California, Berkeley.
- Stewart, J.P., & Stewart, A.F., 1997. Analysis of soil-structure interaction effects on building response from earthquake strong motion recordings at 58 sites. *Earthquake Engineering Research Center*, 97(1).
- Stewart, J., Seed, R. & Fenves, G., 1998. *Empirical evaluation of inertial soil-structure interaction effects*: Pacific Earthquake Engineering Research Center (PEER).
- Stewart, J.P., Fenves, G.L., & Seed, R.B., 1999a. Seismic soil-structure interaction in buildings. I: Analytical methods. *Journal of Geotechnical and Geoenv. Eng.*, 125(1), 26-37.
- Stewart, J.P., Seed, R.B., & Fenves, G.L., 1999b. Seismic soil-structure interaction in buildings. II: Empirical findings. *Journal of Geotechnical and Geoenv. Eng.*, 125(1), 38-48.
- Taciroglu, E., Ghahari, S. & Abazarsa, F., 2015. Efficient model updating of a multi-story frame and its foundation stiffness from earthquake records using a Timoshenko beam model. *Soil Dynamics and Earthquake Engineering* (under review).
- Taciroglu, E. & Ghahari, S., 2015. Identification of Soil-Foundation Dynamic Stiffness from Seismic Response Signals. *ACI Special Publication*.

- Tileylioglu, S., Stewart, J. & Nigbor, R., 2010. Dynamic stiffness and damping of a shallow foundation from forced vibration of a field test structure. *Journal of Geotechnical and Geoenvironmental Engineering*, 137(4), 344-353.
- Timoshenko, S., 1921. On the correction for shear of the differential equation for transverse vibrations of prismatic bars. *The London, Edinburgh, and Dublin Philosophical Magazine and Journal of Science*, 41(245), 744-746.
- Todorovska, M., 2009. Soil-structure system identification of Millikan Library North–South response during four earthquakes (1970–2002): what caused the observed wandering of the system frequencies?. *Bulletin of the Seismological Society of America*, 99(2A), pp. 626-635.
- Veletsos, A. & Verbic, B., 1973. Vibration of viscoelastic foundations. *Earthquake Engineering & Structural Dynamics*, 2(1), 87-102.
- Veletsos, A.S., & Nair, V.V., 1975. Seismic interaction of structures on hysteretic foundations. *Journal of the Structural Division*, 101(1), 109-129.
- Veletsos, A.S., Prasad, A.M., & Wu, W.H., 1997. Transfer functions for rigid rectangular foundations. *Earthquake engineering & structural dynamics*, 26(1), 5-17.
- Wolf, J., 1976. Soil-structure interaction with separation of base mat from soil (lifting-off). *Nuclear Engineering and Design*, 38(2), 357-384.
- Wolf, J. & Deeks, A., 2004. Foundation Vibration analysis: A Strength of Materials Approach. Butterworth-Heinemann.